CURRENT ROUGHNESS OVER SMALL BEDFORMS AND WAVES

M.G. Kleinhans, B.T. Grasmeijer, and B.G. Ruessink
(Utrecht University)

ABSTRACT

Sand grains, bedforms and the wave boundary layer cause roughness for tidal currents. This paper reports roughness and current shear stress in calm weather and storms derived from 1900 hours of detailed flow measurements on a sandy shoreface, 2 km off Noordwijk, The Netherlands. Two methods are employed: fitting logarithmical velocity profiles to data of 3 to 7 sensors, and the inertial subrange method from the spectra collected at 2 Hz. The results are compared to observed bedform dimensions. Various technical problems are discussed. The roughness decreases for increasing current velocity in Hm0 waves <2 m, but increases for larger waves. Individual events show contrasting trends that are probably related to bedform development. Recommendations for future instrumentation and for further analysis of this data are given.

1. INTRODUCTION

Understanding current roughness is relevant for sediment transport modelling on the shoreface. The roughness affects the current magnitude and the sediment stirring, while the current causes most of the net transport when the waves are stirring the sediment (in non-breaking conditions). The causes of roughness are grain roughness, wave-boundary layer thickness (causing apparent roughness) and wave-current bedform or sheet flow roughness (Grant and Madsen, 1982). These add up in some way to a total current roughness, which is, however, notoriously difficult to determine from measurements. The relation between roughness and its causes is therefore far from clear (Houwman and Van Rijn, 1999). Therefore, various methods have been devised to determine roughness, such as the velocity profile method (VPM) and the inertial subrange method (ISM).

The aim of this paper is twofold: to determine the apparent current roughness and study correlations to wave parameters and to compare the two methods. The observed bedforms are described in Dolphin et al. (2005, paper T, this volume) and Kleinhans (2005, paper R, this volume) and bedform types and occurrence in general are described in Kleinhans (2005, paper Q, this volume). First, the field site and methods are described. Second, the results of the VPM are given. Third, the ISM and VPM results are compared. Fourth, the correlation between wave conditions and roughness is determined. After discussing the results and the technical problems, recommendations for future instrumentation and for further analysis of this data are given.

2. FIELD SITE AND METHODOLOGY

The field site is on the Dutch shoreface and shelf in the North Sea, 2 km off Noordwijk at an average water depth of 13 m. Tidal currents are semi-diurnal. The spring-tidal amplitude is 1.3 m and maximum tidal depth-averaged currents are between 0.5-0.7 m s^{-1}. The bed sediment is fine to medium sand with D_{10}=160, D_{50}=216 and D_{90}=288 10^{-6}m.

The hydrodynamics were measured by instruments on three benthic tripods: the Hydro tripod, the Caen tripod and the HSM tripod. The Hydro and Caen tripods have a pressure sensor and 2 or 3 electromagnetic current sensors, respectively, between 0.2-1.2 m above the bed. The HSM tripod has 3 to 7 electromagnetic current sensors between 0.05-1m above the bed and two pressure sensors. All instruments operated in burst mode with a frequency of 2 Hz and a burst duration of 34 minutes. All data were calibrated with calibration slopes from laboratory measurements and offsets measured in the field in a still water bucket immediately before and after the deployments. See Grasmeijer et al. (2005, paper M, this volume) for further details on the data.

The most common method to derive shear stress and roughness from velocity data is the velocity profile method (e.g., Soulsby, 1997), in which the Von Karman logarithmic 'law of the wall' is fitted to at least two velocity measurements at different heights above the bed. This method results in the current shear stress and the current roughness. The latter is sensitive to errors in velocity and height above the bed because it is derived by extrapolation of the measured velocity profile to the level of zero velocity. The law of the wall is:

$$u=u^*\kappa^{-1}\ln(z/z_0) \tag{1}$$

in which u=velocity at height z, z=height above the seabed, u*=shear velocity, κ=Karman constant (0.4) and z_0=height at which u=0. The depth-averaged flow velocity is found at a height of (1/e)h approximated as

0.368h, where h=water depth and e=Euler constant. The Nikuradse roughness length k_s is related to as $k_s=30z_0$. This assumes hydraulic rough conditions, which is the case for Reynolds numbers $Re^*=u^*D_{50}/\nu$ >11.63, in which ν=viscosity and D_{50}=median grain size.

The second method is spectral: the inertial subrange method (Huntley, 1988, Green, 1992). This employs the spectral separation between common frequency ranges for gravity waves and for current turbulence. The energy dissipation far removed from the turbulence-generating length (or time) scales and the turbulence damping length (or time) scale (viscosity) shows up in the double-log spectrum as a -5/3 slope:

$$E(k)=\alpha\, ?^{2/3}k^{-5/3} \tag{2}$$

in which k is the wave number, E(k) is the energy of the one-dimensional spectrum (alongshore velocity) for the applicable inertial subrange, α=0.51 is the one-dimensional Kolmogorov constant (Green 1992) and ? is the energy dissipation rate. The energy in this dissipation range directly relates to the shear stress of the current. This shear stress is then combined with the depth-averaged current from the VPM and the law of the wall to yield roughness. A smooth spectrum was made of alongshore instantaneous velocity of EMF7 (HSM) and EMF2 (Hydro) for each burst with a Hanning window size of 128 samples (4096 total per time series sampled at 2 Hz). The wave part of the spectrum was removed based on the coherence between the velocity and the pressure signal. The part of the spectrum (in double log space) to which a line with slope -5/3 was fitted, is determined by the height of the sensor above the bed, $k_{low}=2\pi/z_{sensor}$, and the size of the sensor, or, in this case, the Nyquist frequency. The shear velocity is now:

$$\hat{u}^*=(?\kappa z_{sensor})^{1/3} \tag{3}$$

in which ? is derived from the fit to the spectrum (equation 2). This estimate has to be corrected using the Reynolds number $Re_c=u^*\kappa z/\nu=3.0\pm0.5\ 10^3$ because below a certain height the inertial subrange is not fully developed (Huntley, 1988):

$$u^*=[\hat{u}^{*3}Re_c\nu/\kappa z]^{1/4} \tag{4}$$

Using this u* and equation 1, the k_s from the ISM is derived. This method is limited to negligible orbital flows, so trends of roughness during storms cannot be studied with the ISM.
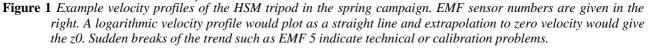
3. RESULTS

3.1 Velocity Profile Method

The velocity profiles for a spring-tidal cycle without waves illustrate the data (Figure 1). The velocities in flood direction are larger than in the ebb direction. There are systematic biases between the EMFs (see discussion), judging from the fact that a logarithmic velocity profile would plot as a straight line.

Figure 1 *Example velocity profiles of the HSM tripod in the spring campaign. EMF sensor numbers are given in the right. A logarithmic velocity profile would plot as a straight line and extrapolation to zero velocity would give the z0. Sudden breaks of the trend such as EMF 5 indicate technical or calibration problems.*
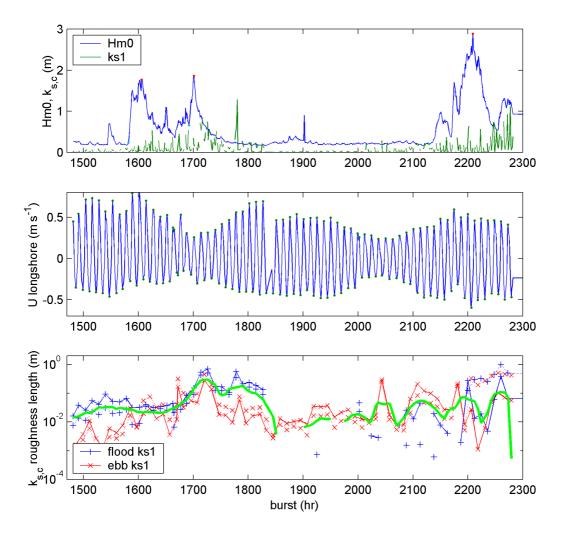
The time series of roughness from the VPM in the spring (Figure 2) and autumn (Figure 3) campaign shows no clear trend with general wave or current parameters. In more detail, the roughness has the lowest value at

peak flows and increases strongly before and after the ebb or flood peak. The roughness of the flood peak is often larger than of the ebb peak.

To test the effect of the number of available EMFs, the data of the spring campaign was processed twice: for EMFs 1, 3 and 7 only (standard case) and for the full dataset. This gives no changes in the trends but a systematic decrease of roughness (Figure 2). The depth-averaged alongshore current velocity is rather insensitive to the amount of sensors and varies only 5-10% (Figure 4a). The roughness, on the other hand, is much more sensitive (Figure 4b). In some parts of the data there is a large deviation (orders of magnitude) for unknown reasons. The depth-averaged current is about 1.25 times EMF7.

Figure 2 *Time series (burst averages) of the spring campaign with the HSM tripod. Top panel gives Hm0 wave height from the pressure sensor and roughness length from EMF 1, 3 and 7. Middle panel gives depth-averaged flow velocity derived from EMF1, 3 and 7. Bottom panel gives roughness length for flood (+) and ebb (x) current peaks from EMF 1, 3 and 7 (-) and from all seven EMF sensors (---).*

3.2 Inertial Subrange Method

Power density spectra were computed for both tripods at exactly the same bursts: 7130-7299. The spectra of the data of the HSM and Hydro tripods are similar, but not equal (Figure 5). The slope of the spectra in the inertial subrange is equal to -5/3 for the Hydro tripod but not for the HSM tripod. Moreover, there appears to be a noise floor near the Nyquist frequency. The height of the spectra, and the burst-averaged velocity of the sensors for the selected spectra, are not the same but this is at least partly explained by the difference in sensor height.

The $u*$ and k_s of the ISM and the VPM are compared (Figure 6). Note that the k_s of the ISM also depends slightly on the depth-averaged current derived from the data with the VPM. The ISM compares moderately well to the VPM for shear velocity and poorly for current roughness. The $u*$ and k_s from ISM of the Hydro

tripod are of the same order of magnitude as from VPM of the HSM tripod, while the ISM of the HSM tripod overestimates the u* a factor of two and the k_s a factor of ten compared to the VPM.
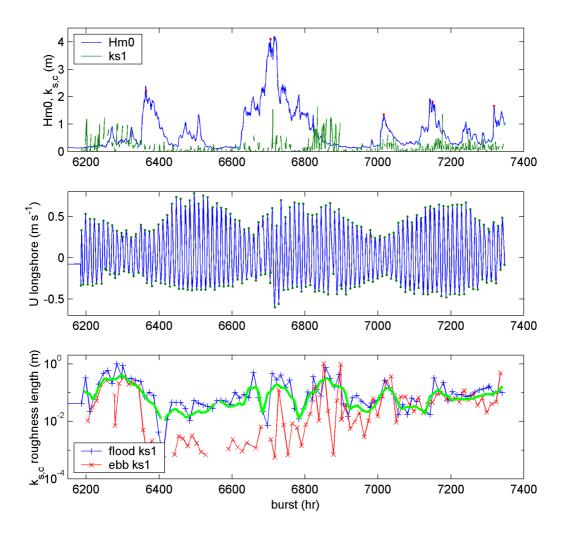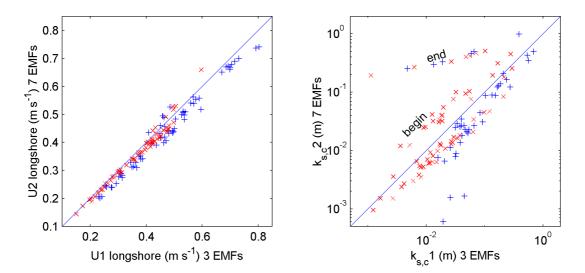

Figure 3 *Autumn campaign with the HSM tripod, as in Figure 2, without roughness for all seven EMF sensors.*

Figure 4 *Comparison of roughness and depth-averaged velocity from velocity profile fitting with all seven EMF sensors and EMF 1, 3 and 7, all from the spring campaign. The deviating roughness are mostly found in the begin and end of the spring campaign, but the reason is not known.*
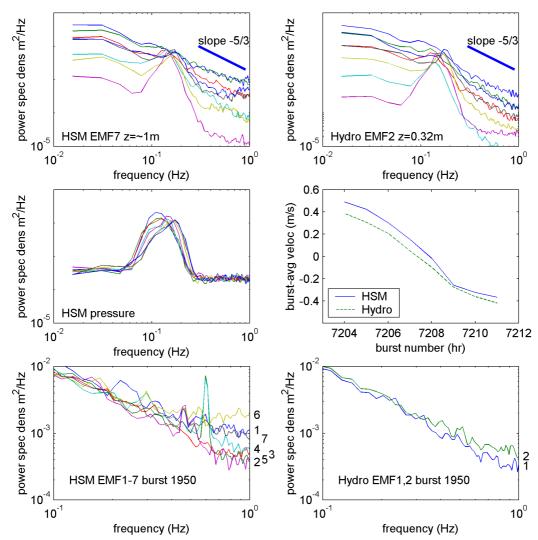
Figure 5 *Power spectral density of the HSM and Hydro tripods of alongshore flow velocity (top panels) and pressure (middle left panel), bursts 7204-7211 (flood peak to ebb peak). The average current velocities of these bursts are given in the middle right panel. The high-frequency part of the spectra of all EMFs for burst 1950 (flood peak in spring during which all EMFs operated) are compared in the bottom panels to demonstrate differences in noise levels (numbers refer to EMF numbers).*
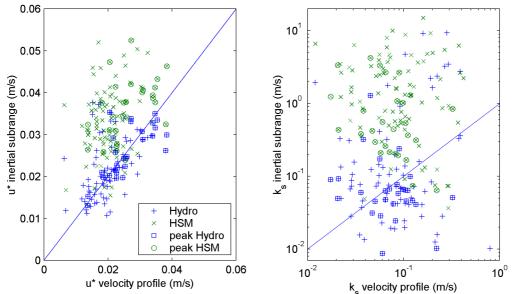

Figure 6 *Comparison of the velocity profile fitting and inertial subrange methods for shear velocity u* and current roughness k_s. Note that the depth-averaged current velocity is needed to derive the roughness for the inertial subrange method.*
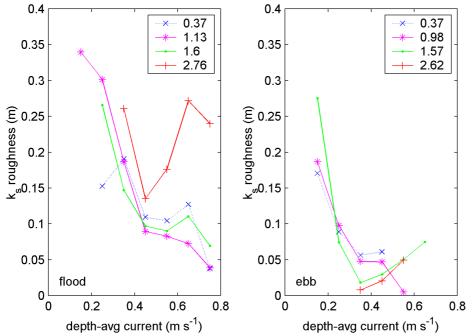
Figure 7 *Moving average of current roughness versus depth-averaged current velocity of the flood and ebb peaks for five classes of wave height Hm0. The largest wave height class (not shown) does not contain enough data.*
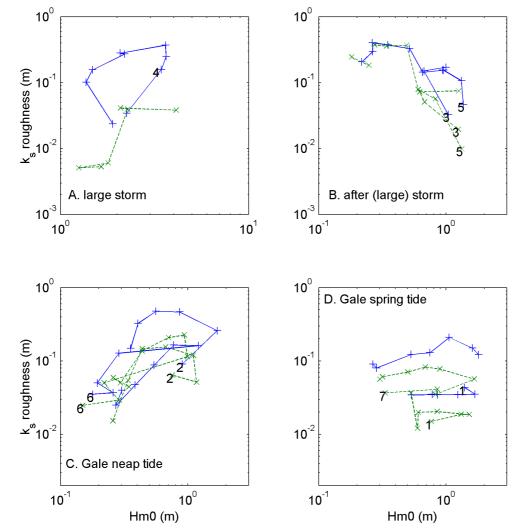

Figure 8 *Smoothed current roughness of flood (+) and ebb (x) current peaks versus wave height Hm0 for four different situations. Numbers are positioned at beginning of time series. A. The large storm in spring tide, bursts 6680-6790 (4). B. After the large storm of A, bursts 6790-6900 (5) and of bursts 2230-2280 (3), also in spring tide. C. Two gales in neap tide, bursts 1680-1760 (2) and 6970-7090 (6). D. Two gales in spring tide, bursts 1580-1660 (1) and 7100-7220 (7).*

3.3 Roughness correlated to waves and physical roughness

There is no general correlation between roughness and wave parameters. There is, on the other hand, a trend of decreasing roughness with increasing depth-averaged current velocity (Figure 7) for roughnesses averaged in current and wave classes and flood/ebb flow peaks. This result was obtained by a moving average of roughness at 0.05 m/s increments of velocity for five overlapping wave height classes of 0-1, 0.5-2, 1-3, 2-4 and 3-7 m. The true average wave heights for each class was computed from the data. The last class did not contain enough data for analysis. The number of points included in each average is at least 3 and at most 50. For $Hm0 < 2$ m, the roughness decreases with increasing current velocity, but for larger waves the roughness *increases* with increasing current velocity, although this trend is uncertain due to the small number of large-storm observations. These trends are similar for ebb and flood current peaks, although the roughness for the largest waves of the flood currents is much larger than of the ebb currents. In addition, there is a robust increase of roughness at about 0.6 m/s (flood) or 0.45 m/s (ebb).

The difference in behaviour for small and large waves is reflected in data of individual events. The roughness now shows a trend with Hm0 wave height, but a different trend for different conditions (Figure 8). A number of situations were extracted from the data with hypotheses on the relations between large waves, bedforms and roughness in mind. The largest storm of the dataset was obviously selected, but also the aftermath of this and another storm. In addition, four minor storms were selected; two in spring-tidal and two in neap-tidal conditions. The aftermath of the storms show an increase of roughness with *decreasing* wave height, whereas the small storms in neap tide show an increase of roughness with *increasing* wave height. The two small storms in spring tide do not show a consistent trend. There is a suggestion of the data following loops through the storm. The loops are anti-clockwise for 2 and 4, but clockwise for 6 and 7. This pattern is similar for flood and ebb current roughness but ebb current roughness is about a factor of two smaller.

4. DISCUSSION

4.1 Technical problems

In general, the EMFs produce good results that are within 1-2% for different tripods, both for burst-averaged currents and for $U_{1/3}$ orbital velocities (Grasmeijer et al., paper M, this volume), even though the tripods are a few hundreds of meters apart. For the determination of roughness, unfortunately, small biases or errors in the data may obscure the trends. This is because roughness determined by the VPM is based on extrapolation, and roughness by the ISM is based on the turbulence part of the spectrum for which the EMFs and the electronics were not designed. Therefore empirical roughness is much more sensitive to such errors than, for example, sediment transport, which is driven by wave stirring and mean currents.

Three technical problems were discovered: 1) there are systematic offsets of several EMFs, 2) the EMFs of the HSM tripod have blue noise over the frequency range suitable for ISM, and 3) the offset and noise of some EMFs of the HSM tripod depend on the orientation of the flow to the tripod. Apart from this, even-numbered EMFs did not work during most of the autumn campaign due to a power supply failure.

The systematic offsets between the EMFs are due to mechanical problems, drag of the tripod legs but also an unknown cause. The EMF with the largest deviation of the lognormal velocity profile (Figure 1) is EMF5, which leaked in most campaigns despite attempts at repair and was therefore excluded from the analyses. Of the six remaining EMFs, it is difficult to say which ones deviate from the others.

The drag of tripod legs is seen when comparing different orientations of the tripod to the flow between the different deployments. For orientations 350-20° (relative to tripod compass direction 0°) EMFs 4, 6 and 7 are in the lee of the ASTM and for 180-210° upstream of the ASTM. The direction of the HSM tripod in the five deployments is 4°, 24°, 255°, 274° and 33°. The direction of the coastline and flood current is 28° and of the ebb current 208°, so none of the deployments is in danger of drag by the ASTM. However, the roughness derived from ebb and flood velocity profiles differs a factor of 10 for the second and fourth deployments. In addition, large differences are found using only EMFs 1,3 and 7 rather than all 1-7 for the spring campaign. Also, only a small number of regressions was significant. These all indicate an orientation-dependent drag effect. In addition, drag from the electronics and batteries may have affected EMF7.

In comparing the Hm0 computed from all the EMFs, systematic differences are found of the order of 5%. This means that not only the mean current but also the local fluctuating components are slightly affected by the aforementioned technical problems. The effect on the spectrum is not known. The blue noise floor in the HSM tripod may be due to the drag effect or to the increased noise in the more compact electronics
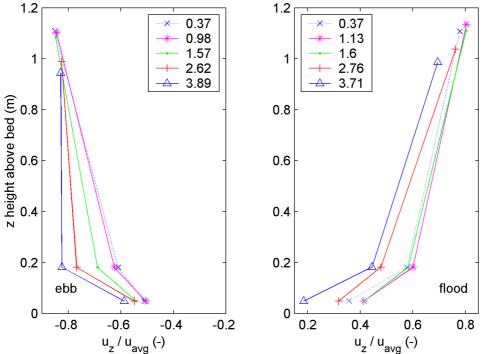
compared to the Hydro tripod. This is why the Hydro tripod data is most suitable for the ISM. In addition, EMF7 is the only working EMF in the suitable height above the bed range for ISM (Figure 5) in the autumn campaign, but EMF7 is suspected of drag from the electronics and batteries.

4.2 Current roughness, wave conditions and physical roughness (bedforms)

There are trends between current roughness and wave conditions (Figure 7) after averaging of the data for velocity and wave height classes. These trends will have to be compared to rotary sonar and ripple profiler data in order to study the relation between roughness and bed state. In addition, models of wave-current interaction will be needed for assessing the wave-added roughness for currents compared to bedform roughness. Nevertheless a tentative interpretation is given of possible relations to expected bedform development.

For small waves the roughness decreases with increasing current velocity, although with a step at 0.6 (flood) or 0.45 (ebb) m/s. For large waves the roughness increases above 0.4 m/s after decreasing for smaller velocities in the same manner as for small waves. This roughness increase for the large waves is already present in the small wave data as the step mentioned above, and is robust for different moving average and classification procedures. This suggests a relation between roughness and bedforms for small waves, and apparent (wave-related) roughness for large waves, although this must be investigated further. Small wave ripples or relic ripples are probably increasingly obliterated by increasing current velocity, which causes a decrease of roughness. Above a certain current velocity and wave height, the total roughness may be increased by wave-current interaction while sheet flow may occur in large waves causing small form roughness. Interestingly, the difference of roughness in ebb and flood currents is probably not an artefact of this dataset. Also Green (1992) and others report this.

A first comparison to real observations of bedforms is done with Figure 2 of Dolphin et al. (2005, paper T, this volume). During storms, long 3D wave ripples are observed and above a wave Shields number of about 0.6 the bed is planed and presumably sheetflow commences. The roughness of wave ripples compared to sheetflow could be much larger so a large roughness is expected for wave ripples and smaller for sheetflow. The present data, however, show larger roughness for larger waves. This may be due to two reasons: the apparent wave roughness becomes dominant in storms, and second, the wave ripple crests are roughly parallel to the current.

Figure 9 *Nondimensional velocity profiles of flood and ebb current peaks of subclasses of depth-averaged velocity u_{avg} (see Figure 7): for flood 0.55< u_{avg}<0.75 m/s and for ebb -0.45< u_{avg}<-0.25 m/s for different wave classes (average Hm0 of each class in the legend). Due to the larger current velocity classes than in Figure 7 the data for the largest waves could also be averaged, resulting in an extra wave height class.*

For individual events contrasting trends were observed (Figure 8), which explains the lack of a singular correlation. In the large storm (Figure 8a) there are also spring tidal currents, so a current bedform may cause

the large roughness in waves which on their own would cause sheet flow. In addition, added apparent roughness due to the waves may cause the large roughness. In the aftermath of the storms (Figure 8b), wave ripples may emerge, possibly on top of current bedforms. For much smaller storms in spring tide (gales, Figure 8c), also wave ripples may emerge in rising wave heights, although the wave heights are much smaller than in the large storm. Possibly the sediment mobility is raised by the spring-tidal currents. For two comparable small storms in neap tide (Figure 8d) this trend is not obvious. Sudden jumps in roughness at large wave heights suggest a transition to or from sheet flow in storms 4 and 7.

A similar conclusion must be drawn for the relation between bedforms and roughness individual storms (Figure 2 of Dolphin et al. and Figure 8 herein). In the largest autumn storm (bursts ~6700) sheetflow occurs, but the roughness remains large which cannot be explained from the bedform type only. A more detailed analysis of the bedform observations may be needed.

The average velocity profiles are clearly changed by larger roughness (Figure 9). For the selected ebb current peaks ($-0.45 < u_{avg} < -0.25$ m/s), the smallest roughness occurs with the largest waves and causes the strongest curvature. For the selected flood current peaks ($0.55 < u_{avg} < 0.75$ m/s), the largest roughness occurs with the largest waves and causes the strongest decrease of velocity in the first meter above the bed.

There is barely enough data for a classification in wave classes, current classes and wave-current angle classes, but the moving average suggests that waves opposing the current cause the largest roughness (Figure 10). Moreover, this roughness does not decrease for wave Shields numbers above unity at which sheet flow occurs (Dolphin et al., this volume).
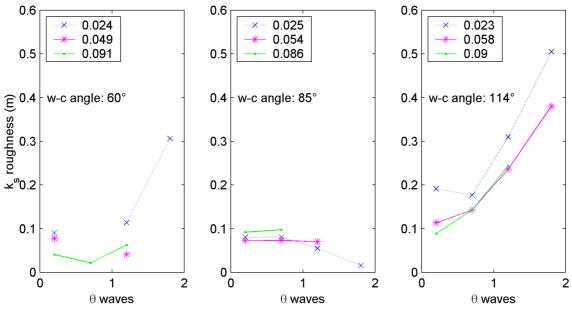

Figure 10 *Roughness for classes of current and wave Shields numbers and the angle between currents and waves. The legend contains Shields numbers of the current.*

5. CONCLUSIONS

To measure current roughness in field conditions, two methods were compared: the velocity profile method (VPM) and the inertial subrange method (ISM). The latter is not applicable to currents plus waves. The shear velocity for the two methods is comparable, but the roughness is much more sensitive to scatter and is not comparable except in magnitude.

Two technical problems affect the offset and noise of the velocity sensors. The first is offsets (after proper calibration), which affect the VPM results and is probably the result of drag from tripod legs and batteries. The second is blue noise in the HSM-tripod compared to the Hydro-tripod, which affects the ISM results.

The roughness is decreases with current velocity for Hm0<2 m and increases for larger waves. Individual events show contrasting trends which are possibly related to bedform dynamics (to be studied further). However, the roughness in the sheetflow regime is large as well. Roughness of the current with opposing waves is larger than for following waves, while the perpendicular cases give the smallest roughness.

6. RECOMMENDATIONS

We recommend for future instrumentation:
- use an array velocity instrument (e.g. down-looking ADCP with small bins?) to overcome bias due to individual instrument offsets and identify possible drag effects
- make the tripod more open than the HSM in all directions, especially that of the current
- test the tripod not only in a large wave flume but also a large current flume or river
- the velocity measurements should span at least the lower 1.5 m of the water column down to 0.01 m above the bed; for good profiles not only good near-bed measurements are needed but also further up
- isolate the electronics of this instrument from other electronics to reduce noise and sample at at least 4 Hz for better turbulence measurements

We plan the following data analyses of this dataset:
- compare bedform development to roughness development
- use the total turbulent kinetic energy method (Soulsby 1997) to derive shear stress and compare that to the inertial subrange method
- model intrawave near-bed flows with measured forcing (velocity time series) and turbulence closure (Houwman, 2000, Houwman and Ruessink, in prep., Grasmeijer et al., 2005, paper U, this volume) for comparison, and derive both modelled and alternative shear stress and roughness values from the model output with the same methods as for the field data

7. REFERENCES

Dolphin, T. , Grasmeijer, B.T. and Vincent, C.E. 2005. Sand suspension due to waves and tidal flow over short and long wave ripples, and flat beds on the Dutch shoreface. This volume, paper R.

Grant, W.D. and Madsen, O.S. 1982. Movable bed roughness in unsteady oscillatory flow. J. of Geophysical Research 87(C1), 469-481.

Grasmeijer, B.T., Kleinhans, M.G., Dolphin, T., van Rijn, L.C., Doucette, J.F. and van der Werf, J.J. 2005. Database of field and laboratory measurements. This volume, paper M.

Green, M.O. 1992. Spectral estimates of bed shear stress at subcritical Reynolds numbers in a tidal boundary layer. J. Physical Oceanography 22, 903-917.

Houwman, K.T. 2000. Tide, wind- and wave-driven flow processes in the nearshore zone. Utrecht University, Faculty of Geography, Utrecht, The Netherlands.

Huntley, D.A. 1988. A modified inertial dissipation method for estimating seabed stresses at low Reynolds numbers, with application to wave-current boundary layer measurements. J. Physical Oceanography 18, 339-346.

Kleinhans, M.G. 2005. Bedforms and mud dynamics on the shoreface and upper shelf, Noordwijk, The Netherlands. This volume, paper R.

Kleinhans, M.G. 2005. Phase diagrams of bed states in steady, unsteady, oscillatory and mixed flows. This volume, paper Q.

Soulsby, R. 1997. Dynamics of marine sands. Thomas Telford Publications, London, United Kingdom.

8. ACKNOWLEDGEMENTS